Modeling the Impacts of Land Use Changes on Soil Erosion at the River Basin Scale

Xiong, Yanna
State Key Laboratory of Environmental Criteria and Risk Assessment, Chinese Research Academy of Environmental Sciences

Wang, Guoqiang
College of Water Sciences, Beijing Normal University, Engineering Research Center of Groundwater Pollution Control & Remediation, Ministry of Education

Teng, Yanguo
College of Water Sciences, Beijing Normal University, Engineering Research Center of Groundwater Pollution Control & Remediation, Ministry of Education

Otsuki, Kyoichi
Laboratory of Ecohydrology, Division of Forest Sciences, Department of Agro-environmental Sciences, Faculty of Agriculture, Kyushu University

https://doi.org/10.5109/27370

出版情報：九州大学大学院農学研究院紀要. 58 (2), pp.377-387, 2013-09. Faculty of Agriculture, Kyushu University
バージョン：
権利関係：

J. Fac. Agr., Kyushu Univ., **58** (2), 377–387 (2013)

Modeling the Impacts of Land Use Changes on Soil Erosion at the River Basin Scale

Yanna XIONG[1, 2], Guoqiang WANG[1]*, Yanguo TENG[1] and Kyoichi OTSUKI

Laboratory of Ecohydrology, Division of Forest Sciences, Department of Agro–environmental Sciences, Faculty of Agriculture, Kyushu University, Sasaguri, Fukuoka 811–2415, Japan
(*Received April 25, 2013 and accepted May 9, 2013*)

The potential for soil erosion is strongly affected by land use. A proper modeling approach should be selected to explicitly assess the impacts of land use changes on soil erosion at a river basin scale. The reliability of simulation results from erosion models is circumscribed by considerable spatial variation in many parameters. In this study, a grid–based distributed soil erosion and sediment transport model was used in conjunction with a laboratory rainfall simulation experiment to determine the impact of land use changes on soil erosion and sediment yield in a river basin during individual storms. Land use changes in the Lushi Basin, primarily in Henan, China, were analyzed by comparing the historical land use maps in 1990 and 1995. Through comparing the results for four selected storms that were compiled using these two land use maps, it was found that the average erosion rates increased from 1989 to 1996. The increase in average erosion rates followed the land use changes, especially the transformation of forest to farmland. The results indicated that even slight land use change, from forest to farmland or vice versa, had a significant effect on regional soil erosion rates and sediment supply to rivers.

Key words: rainfall simulation, sediment, soil erosion

INTRODUCTION

Soil erosion is a very serious environmental concern as it removes soil rich in nutrients and increases the level of sedimentation in rivers, which reduces the life span of the river channel. Natural as well as human–induced land use change has significant impacts on regional soil erosion. Since the last century, human activities often tended to accelerate soil erosion creating serious environmental problems. Soil erosion has a manifold environmental impact by negatively affecting water supply, reservoir storage capacity, agricultural productivity, and fresh water ecology of the region (Sharma *et al*., 2011). In China, soil erosion affects an area of about 3.6×10^6km^2, covering nearly 37% of the total land area of the country. Among all the erosion affected regions, the Yellow River basin, and especially the middle reach, contributes more than 30% of the total soil loss in China. Human impact, such as land use changes, was found to be the dominant factor in affecting soil erosion rates in this region (Ni *et al*., 2008). Similarly, many researchers (Toy *et al*., 2002; Houben *et al*., 2006) have found that changes in land use and climate were two important factors affecting soil erosion and sediment delivery to rivers. In recent years, many studies concerning soil erosion focused on the effect of global change, especially the effect of climate change, on erosion at the basin scale (Nicks *et al*., 1994; Favis–Mortlock and Boardman, 1995). Also, Ludwig *et al*. (1995) and Singh *et al*. (2012) found that land use change had the same important roles in altering soil erosion potential in river basins. One way to assess the impact of land use change on soil erosion involves using historic satellite images to analyze land use in relation to change in soil erosion potential of basin or sediment discharges at basin outlets (Jordan *et al*., 2005). In recent years, a number of studies have been carried out to estimate the effects of land use change on soil erosion at different spatiotemporal scales (Pruski and Nearing, 2002; Dunjo *et al*., 2004; Jordan *et al*.,2005; Jain and Das, 2010; Chou, 2010). All these studies verified the strong influence of land use changes on soil erosion and sediment yield. Since the land use patterns were expected to change because of human activities in the future, it is important to examine the potential effects of these changes on soil erosion at basin scale through a modeling approach.

Regional scale soil erosion estimates are influenced by complex soil erosion processes and the availability of data describing the soil erosion factors. In the last decade, regional and national level assessments of soil erosion were carried out using different approaches, ranging from indicator or factor–based approaches to process–based models (Sharma *et al*., 2011). Among the approaches, the Universal Soil Loss Equation (USLE) (Wischmeier and Smith, 1978) and its revised version, RUSLE, (Renard *et al*., 1997) represent the most widely used method for estimating long–term soil loss despite the fact that these methods have several shortcomings. Other more process–based models such as the Water Erosion Prediction Project (WEPP) (Nearing *et al*., 1994) and EUROSEM (Morgan *et al*., 1998) are available; however, these models are often too data and computationally intensive to use in many circumstances, particularly in respect to modeling soil erosion in large basins. The USLE approach holds the advantage in such

[1] College of Water Sciences, Beijing Normal University, Engineering Research Center of Groundwater Pollution Control & Remediation, Ministry of Education, Beijing 100875, China
[2] State Key Laboratory of Environmental Criteria and Risk Assessment, Chinese Research Academy of Environmental Sciences, Beijing 100012, China
[3] Kasuya Research Forest, Kyushu University, Sasaguri, Fukuoka 811–2415, Japan
* Corresponding author (E–mail: wanggq@bnu.edu.cn)

circumstances because of a perceived ease of parameterization and use. Although originally developed as an empirical model, revisions of the USLE could lead to a more conceptual model that provides a capacity to extend well its use beyond the conditions experienced in the associated data set (Kinnell, 2005). Ricker *et al.* (2008) analyzed the spatial distribution of soil erosion and sediment fluxes in two tributaries of the Rappahannock River using a combined RUSLE/SDR (Sediment Delivery Ratio) method. While the combined RUSLE/SDR considered sediment transport, the RUSLE was still found to overestimate the low levels of soil erosion occurring when the soil surface has a high capacity to allow rainfall to infiltrate (Risse *et al.*, 1993) although the degree of overestimation falls as the capacity of the soil to produce surface runoff increases. An important reason behind the overestimation is the lack of a runoff factor in the USLE. Kinnell (2003) designed the USLE–M model which solved this limitation by incorporating an event erosivity factor.

This paper presents a modeling structure that allows assessment of the effect of land use changes on soil erosion. Laboratory rainfall simulation experiments were also conducted in this study. The experimental data were analyzed to process the soil related parameters, especially the soil erodibility factor, for the erosion model. The erosion model emphasizes a good prediction of soil erosion patterns and an integration of different erosion types while process description is rather simple. The erosion model was verified to be capable of modeling the impact of land use changes on soil erosion through a case study in the Lushi Basin, China.

MATERIALS AND METHOD

Study area

The Luo River drains the Lushi Basin, a mid–basin tributary of the Yellow River mostly within Henan, on China's mainland (see Fig. 1). The 4,423 km^2 basin has 31 rain gauging stations located along the river. The discharge gauging station at the Lushi site lies at the outlet of the basin. Annual precipitation in the Lushi Basin averaged 703 mm from 1971 to 1996. Lushi Basin suffers from severe erosion problems caused by the concentrated rainfall characteristics and the land use changes in this region. About 60% of the annual precipitation is concentrated in numerous rainstorms during the rainy season from June to September. Hourly precipitation data recorded at the 31 rain gauging stations and hourly discharge data recorded at the Lushi site are available for this study (Wang *et al.*, 2010). The topographic characteristics of the Lushi Basin were extracted using Shuttle Radar Topography Mission DEM (Digital Elevation Model) data. The DEM data in Lushi Basin allowed generation of a mean slope of about 11 degrees, although about 7% of all the grids have slopes greater than 25 degrees.

The land use patterns of Lushi Basin were relatively stable in the 1970s and 1980s, while they changed rapidly since the 1990 as a result of rapid economic growth in this region. Based on the land use maps interpreted from Landsat 5 Thematic Mapper (TM) data in 1990 and 1995 (see Fig. 2), the dominant land use type in the basin was several types of forests (51% of the total area) followed by grasslands (28%) and farmland (21%).

The erodible nature of Lushi Basin soils aggravates erosion problems. Soils in the basin were identified from the Chinese national 1:4,000,000 scale soil map provided by Chinese Academy of Sciences (see Fig. 3) and were classified into two major types. The major soil types are

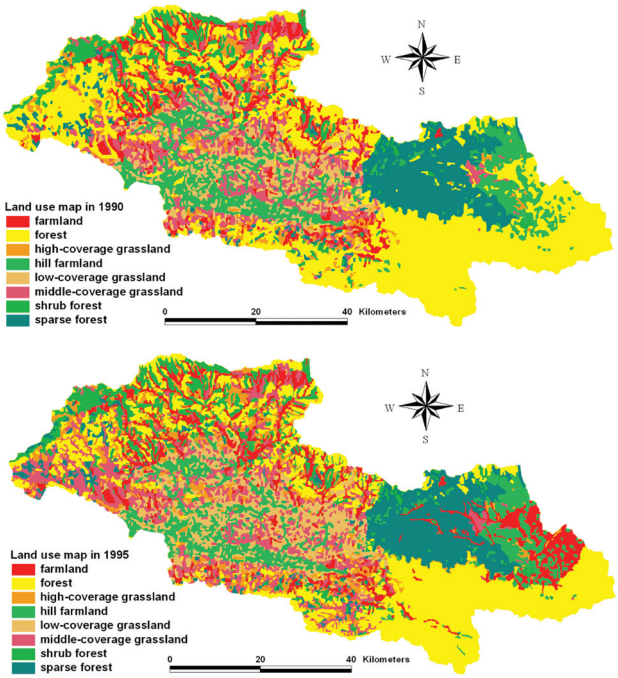

Fig. 2. Land use map of the Lushi Basin in 1990 and 1995.

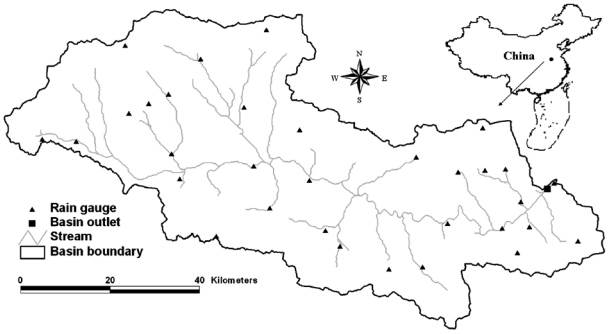

Fig. 1. Map of the Lushi Basin, China.

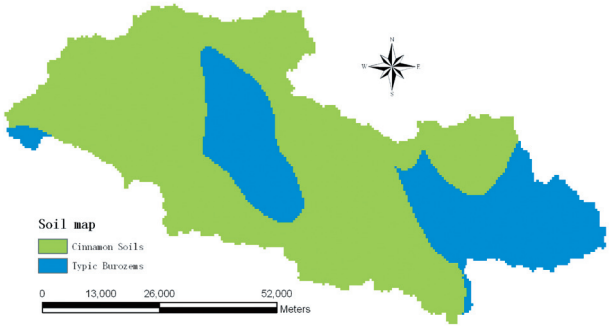

Fig. 3. Soil map of the Lushi Basin.

zonal from areas with elevations ranging from up to 3,500 m down to about 400 m, changing from the Cinnamon Soils, which cover about 70% of the basin to Typic Burozems making up the other roughly 30% (Hao *et al*., 2004).

Numerical modeling of rainfall–runoff

Understanding the surface and subsurface characteristics that drive the mechanisms for runoff and soil erosion is required to explicitly describe the erosion process. In this study, the erosion modeling is integrated with a grid–based distributed hydrological model, BTOPMC (Block–wise use of TOPMODEL), which simulates the rainfall–runoff process and generates hydrologic inputs for the erosion model. The BTOPMC model was developed for hydrological simulations for the meso– and large–scale river basins (Takeuchi *et al*., 1999; Wang *et al*., 2007). In this model, runoff generation is based on TOPMODEL (Beven *et al*., 1995) and flow routing is carried out by the Muskingum–Cunge method (Ao *et al*., 2000). Drainage networks are generated using the automated pit–removal method (Ao *et al*., 2001).

BTOPMC defines the soil profile as having three vertical zones; a root zone, an unsaturated zone and a saturated zone. Similarly to TOPMODEL, BTOPMC is based on the saturation excess runoff mechanism. Wang *et al*. (2007) further improved the BTOPMC model by incorporating an infiltration model that combines the Philip (1957) equation with the time compression approximation (TCA) method (Sherman, 1943). Under the new model structure, Hortonian flow $q_{ofh}(t)$ (m h^{-1}) occurs if the infiltration rate $f^*(t)$ (m h^{-1}) is less than the rainfall intensity I_t (m h^{-1}).

$$q_{ofh}(t)=\max\left\{I_t-f^*(t),\,0\right\} \tag{1}$$

The infiltrated rainfall enters the root zone and changes its soil water content $S_{rz}(t)$ (m) to:

$$S_{rz}(t)=S_{rz}(t-1)+f^*(t)\cdot\Delta t \text{ subject to } 0\le S_{rz}(t)\le S_{r\max} \tag{2}$$

where S_{rmax} (m) is the maximum water storage of the root zone. Once S_{rmax} is reached, more infiltrated rainfall leads to a storage excess in the root zone, $EX(t)$ (m), that drains into the unsaturated zone under gravity.

$$EX(t)=[S_{rz}(t-1)+f^*(t)\cdot\Delta t-S_{r\max} \text{ subject to } EX(t)\ge 0 \tag{3}$$

The unsaturated zone is reclassified from an inactive area to an active area. The field capacity in the inactive area is static, while the active area receives excess water from the root zone and fills the unsaturated zone storage $S_{uz}(t)$ (m). Meanwhile, water in the unsaturated zone drains into the saturated zone at a rate $q_v(t)$ (m h^{-1}).

$$S_{uz}(t)=S_{uz}(t-1)+EX(t)-q_v(t)\,\Delta t \text{ subject to } S_{uz}\ge 0 \tag{4}$$

The recharge rate to the saturated zone $q_v(t)$ (m h^{-1}) can be calculated as:

$$q_v(t)=K_s\exp[-SD(t)/m_0] \text{ if } q_v(t)\cdot\Delta t\le S_{uz}(t) \tag{5}$$

where $SD(t)$ (m) is the saturation deficit in the unsaturated zone, K_s (m h^{-1}) is the saturated hydraulic conductivity and m_0 (m) is a parameter describing the exponential decay in the transmissivity of the soil column. The saturation deficit can be calculated from:

$$SD(t)=\overline{SD}(t)+m_0(\overline{\gamma}-\gamma-\overline{\ln D_0}+\ln(D_0)) \tag{6}$$

where $\overline{SD}(t)$ (m) is a block average of saturation deficit, γ is a topographic index, D_0 (m h^{-1}) is the soil water transmissivity, $\overline{\gamma}$ and $\overline{\ln D_0}$ are the block average values of γ and $\ln(D_0)$.

$$D_0=U_{clay}D_{clay}+U_{sand}D_{sand}+U_{silt}D_{silt} \tag{7}$$

where U_{clay}, U_{sand} and U_{silt} are the percentages of clay, sand and silt present in the particular grid cell, respectively. Since soil texture inside a grid is assumed to be homogeneous, the coefficients of D_{clay}, D_{sand} and D_{silt} could represent additional soil textural properties. $\overline{SD}(t)$ (m) is obtained from:

$$\overline{SD}(t+1)=\overline{SD}(t)-[\overline{q_v}(t)-\overline{q_b}(t)]\cdot\Delta t-[\overline{S_{uz}}(t)-\overline{S_{uz}}(t-1)] \tag{8}$$

where q_b (m h^{-1}) is the base flow, and $\overline{q_v}(t)$ (m h^{-1}), $\overline{q_b}(t)$ (m h^{-1}) and $\overline{S_{uz}}(t)$ (m h^{-1}) are the spatially averaged $q_v(t)$, $q_b(t)$ and $S_{uz}(t)$ values in a block, respectively.

If water recharge to the unsaturated zone exceeds the saturation deficit $SD(t-1)$ (m), the additional portion of the water recharge is considered to be the saturation excess overland flow q_{of} (m h^{-1}).

$$q_{of}(t)\,\Delta t=EX(t)+(q_v(t)-q_b(t))\,\Delta t-SD(t-1) \tag{9}$$

In the saturated zone, the soil moisture content does not change. However, the saturated zone receives recharge water from the unsaturated zone and releases a base flow. $q_b(t)$ (m h^{-1}) is represented as:

$$q_b(t)=D_0\tan\beta\exp[-SD(t)/m_0] \tag{10}$$

where $tan\,\beta$ is the hydraulic gradient of the saturated zone.

Numerical modeling of soil erosion

Defining the critical conditions needed for rill occurrence is usually difficult. In this study, instead of simulating interrill erosion and rill erosion separately, the two erosion types are lumped together and simulated by the USLE–M model, which was improved from USLE by redefining the equation factors (Kinnell, 1997).

The classic USLE method was developed to estimate event level soil loss A (kg m^{-2}) using rainfall, soil, land use, topographic and management practice data. A can be estimated as:

$$A=R\cdot K\cdot L\cdot S\cdot C\cdot P \tag{11}$$

where R (MJ mm m^{-2} h^{-1}) is the rainfall erosivity factor, K (kg h MJ^{-1} mm^{-1}) is the soil erodibility factor, L is the slope length factor, S is the slope gradient factor, C is the cover management factor and P is the support practice factor. The factors L, S, C and P are unitless and dimensionless. The primary factor in USLE, the R factor, is the product of storm rainfall energy and the maximum 30–minute rainfall intensity I_{30} (m h^{-1}). In RUSLE2 (Daniel *et al.*, 2003), the traditional USLE structure has been verified as being applicable under stepwise rainfall, and the R factor for a particular event is then described as the sum of the stepwise R_t (MJ mm m^{-2} h^{-1}) factors that are derived from a function of the energy per unit rainfall amount e_t (MJ m^{-3}), I_t (m h^{-1}) and I_{30} (m h^{-1}).

$$R=\sum_{t=1}^{T} R_t=\sum_{t=1}^{T} e_t\cdot I_t\cdot \Delta t\cdot I_{30} \tag{12}$$

where T represents the time steps in an event. While in USLE–M, a storm erosivity factor (R_e) is proposed based on the concept that event erosion is given by the product of runoff amount and bulk sediment concentration for the event (Kinnell, 1997). Therefore, R_e (MJ mm m^{-2} h^{-1}) can be represented as:

$$R_e=Q_R R=\sum_{t=1}^{T}(Q_R)_t\cdot R_t \tag{13}$$

where Q_R is the runoff ratio and $(Q_R)_t$ reflects the runoff ratio during time step t. Q_R is a reduced variable that varies between 0 and 1, which can be calculated from the BTOPMC model.

The inclusion of direct consideration of an event runoff in the R_e factor improves the capacity of the USLE–M to simulate event erosion (Kinnell, 2003). However, as with USLE, the USLE–M is an empirically derived model. Changing the erosivity factor leads to a concern that the same parameter values for other factors may not be directly used, especially the K factor, which is tightly related to the integrated effect of rainfall, runoff and infiltration on soil loss. In USLE–M, the event erodibility factor K_e (kg h MJ^{-1} mm^{-1}) is determined from runoff and soil loss experiments on bare plots as:

$$K_e=\frac{\sum_{j=1}^{n} A_j}{\left(\sum_{j=1}^{n} R_{e,j}\times LS\right)} \tag{14}$$

where A_j (kg m^{-2}) and $R_{e,j}$ (MJ mm m^{-2} h^{-1}) represent the plot–measured A and R_e factor values, respectively. j represents storm event and n is the number of storm events. In this study, rainfall simulation experiments were conducted in designed soil flumes to measure the K_e factors for the dominant soil types in the study area.

The grid–based description of the L factor proposed by Kinnell (2005) is used, which improves the Desmet and Gover method (1966) by distinguishing actual runoff from storm rainfall in determining the L factor. This gives an approach to describing the L factor that is consistent with calculating the R_e and K_e factors. Thus, the L factors can be estimated for a grid as:

$$L=\frac{Q_{rO}(a+d^2)^{m+1}-Q_{in}a^{m+1}}{P_u(22.13)^m d^{m+2}x^m} \tag{15}$$

where Q_{ro} (mm^{-2}) is the runoff passing across the lower boundary of a grid cell, Q_{in} (mm^{-2}) is the runoff passing across the upper boundary, d (m) is the length of a grid cell, a (m^2) is the upstream basin area of a grid cell, P_u (mm^{-2}) is rainfall amount per unit area during the event, x is a factor that is dependent on flow direction and m is the slope length exponent. The equation enables the USLE–M model to account for the effect of variations of runoff in terms of determining the slope length factor. The S, C and P factors in USLE–M are determined in the same way as in USLE. The sediment transport process is described using one–dimensional continuity equation of sediment mass in the surface flow regime (Wang *et al.*, 2010). The continuity equation is given as:

$$\frac{\partial q_s}{\partial x}+\rho_s\frac{\partial(c_s h)}{\partial t}=D_s \tag{16}$$

where q_s (kg h^{-1} m^{-1}) is the sediment discharge per unit width of flow, h (m) is the water depth of channel flow, ρ_s (kg m^{-3}) is the mass density of sediment particles, c_s (m^3 m^{-3}) is the sediment concentration by volume and D_s (kg h^{-1} m^{-2}) is the sediment detached from the grid. D_s includes both interrill and net rill erosion rates and is calculated using the USLE–M equation. The $\partial q_s/\partial x$ term represents the change in sediment flow rate along a slope and $\rho_s\partial(c_s h)/\partial t$ represents the change in sediment storage over time. The sediment transport process is controlled by both the amount of sediment available for transport and the transport capacity of the flow. Deposition of sediment occurs if the sediment load exceeds the transport capacity of the flow. Beasley *et al.* (1980) compared different relationships for transport capacity and suggested simplified formulations for two–stage transport capacity as a function of discharge Q_{ch} (m^3 h^{-1} m^{-1}) and slope $\tan\beta$ for laminar and turbulent flows. Transport capacity of flow T_c (kg h^{-1} m^{-1}) is calculated from:

$$T_c=\begin{cases} 161\tan\beta\cdot Q_{ch}^{0.5} & \text{for } Q_{ch}\le 2.76\,(\text{m}^3\text{h}^{-1}\,\text{m}^{-1}) \\ 16320\tan\beta\cdot Q_{ch}^{2} & \text{for } Q_{ch}\le 2.76\,(\text{m}^3\text{h}^{-1}\,\text{m}^{-1}) \end{cases} \tag{17}$$

Erodibilty experiment at laboratory using rainfall simulation

Laboratory rainfall simulation experiments were conducted to quantify a number of erosion related parameters under certain controlled conditions, such as erodibility and soil water content. Of all these parameters, event soil erodibility factor K_e was found to affect soil erosion estimation significantly. In this study, the K_e factor was obtained for the model simulation from these labo-

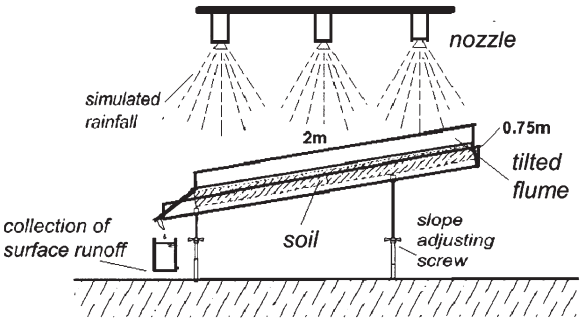

Fig. 4. Schematic map of the rainfall simulation.

ratory rainfall simulation experiments. The experiments were carried out using a soil flume and a rainfall simulator. The schematic representation of the experimental setup is presented (Fig. 4).

The soil flumes were constructed with 2.0 m long × 0.75 m wide × 0.5 m tall metal sheets. Surface runoff and drainage water were collected at the end of the flume. Since slope is one of the critical factors controlling soil erosion by overland flow (e.g., Bryan and Poesen, 1989), the structure had slope adjusting screws allowing the control of the flume slope.

Surface layers of Cinnamon and Burozem soil, soils with similar properties, were collected from Lushi Basin for the experiment. The initial soil properties of the two soil samples are provided in Table 1. After collection, the soil was processed using standard procedures involving pre–sieving through a 4.75 mm aperture square–hole sieve to remove coarse rock and organic debris. The soils were uniformly spread in the flumes, followed by gently taping with a wooden block and scraping the surface to a uniform thickness of 0.4 m, aiming to attain uniform densities matching the initial densities of the sampled soils.

The rainfall simulator was used to generate precipitation with varying intensities, which consisted of three groups of oscillating TSPT–X type nozzles. The rainfall simulator was a 3–nozzle unit that in design, principle of operation, and characteristics, was similar to the multiple–intensity rainfall simulator described by Romkens *et al.* (2001). The properties of storms generated with this rainfall simulator were very similar to those of natural storms of corresponding intensity. On each soil flume, 40 min rainfall simulation events were conducted at two intensities, 60 and 120 mm h^{-1}. Similar simulation events were done for two bed slopes (10 and 20%). Prior to each simulation, the soil water content in the soil flume was adjusted to the same levels of soil samples through operating the simulator at low rainfall intensities and the bulk densities were quantified. During each simulated rainfall event, runoff at the outlet was measured and sampled at 5–minute intervals. Runoff sediment concentration was determined by oven drying at 105°C, total surface runoff and sediment amounts of each simulated rainfall event were then calculated (Table 2).

Dataset

Preliminary examinations of the rainfall, discharge and sediment concentration data integrities in time series allow the identification of 29 events recorded from 1971 to 1996. The rainfall data recorded at 31 rainfall gauging

Table 1. Soil properties of two soil samples collected from the study area

Soil Type	Mechanical composition (%)				Bulk density (g cm^{-3})	Soil water content (%)	pH	Organic matter (g kg^{-1})
	>0.1 mm	0.1–0.05 mm	0.05–0.01 mm	<0.01 mm				
Burozems	45.33	31.40	19.94	3.32	1.32	3.68	6.7	8.66
Cinnamon soils	9.05	56.97	24.98	8.99	1.65	5.77	6.5	10.22

Table 2. Soil experimental conditions and observed results from the rainfall simulation experiments

Soil type	Slope	Rainfall intensity (mm h^{-1})	Surface runoff (mm)	Q_R	A (kg m^{-2})	$\sum A$ (kg m^{-2})	R (MJ mm m^{-2} h^{-1})	R_e (MJ mm m^{-2} h^{-1})	LS	$\sum R_e LS$ (MJ mm m^{-2} h^{-1})	K_e (kg h MJ^{-1} mm^{-1})
Burozems	10%	60	18.1	0.45	0.14	1.54	0.07	0.03	0.35	0.23	6.69
		120	30.0	0.38	0.40		0.28	0.11			
	20%	60	28.3	0.71	0.43		0.07	0.05	1.05		
		120	34.6	0.43	0.57		0.28	0.12			
Cinnamon soils	10%	60	28.6	0.72	0.21	2.08	0.07	0.05	0.35	0.32	6.50
		120	37.1	0.46	0.55		0.28	0.13			
	20%	60	33.2	0.83	0.64		0.07	0.06	1.05		
		120	52.6	0.66	0.68		0.28	0.18			

stations were interpolated using the Thiessen polygon method. Discharge and sediment concentration data were recorded at the basin outlet station at the Lushi site. Hourly sediment flux was then obtained by multiplying hourly river discharge by sediment concentration. The numerical modeling was operated in hourly time steps, and used for identifying the regions with high erosion potential and assessing the effect of land use changes on soil erosion. Two land use maps in 1990 and 1995 were used in the simulations to distinguish the effects of land–use change on soil erosion. Since the land use patterns of Lushi Basin were relatively stable in 1970s and 1980s, the land use map in 1990 was used for the events recorded from 1971 to 1989. The land use map in 1995 was used for the events recorded from 1991 to 1996.

Model calibration and validation

The numerical soil erosion model was calibrated and validated using the observed discharge and sediment yield data at 500 m spatial resolution. The model parameters were calibrated manually based on the physical basin features of land cover, soil, etc. Four storm events recorded between 1971 and 1973 were used for model calibration and the other recorded storm events were used for model validation. The Nash–Sutcliffe (*Nash*) coefficient of efficiency (Nash and Sutcliffe, 1970) was used as the objective function for optimizing the model performance. *Nash* is defined as:

$$Nash = 1 - \sum_{i=1}^{n}(Q_{oi} - Q_{si})^2 \Big/ \sum_{i=1}^{n}(Q_{oi} - \overline{Q}_o)^2 \qquad (18)$$

where Q_{oi} ($m^3\ s^{-1}$) is observed discharge, Q_{si} ($m^3\ s^{-1}$) is simulated discharge, n is the total number of records for comparison, and $\overline{Q}_o$($m^3\ s^{-1}$) is the mean value of the discharge observed over the simulation period. The model involved several parameters, of which the parameters subjected to calibration were divided into two groups responsible for runoff and soil erosion simulations, with the parameters related to the latter calibrated first (Table 3). In this study, K_e factor was assigned with values derived from the laboratory experiments, C factor was initialized using the recommended values in USLE and then calibrated according to the land use types (Table 4), and the P factor was assigned the value of 1.0 for the entire basin. Of the initial conditions, the initial soil water content was important for simulating both runoff and soil erosion and its values varied from event to event depending on the initial condition settings. In this study, the initial soil water content value was adjusted slightly for the simulations during model calibration.

RESULT AND DISCUSSION

Estimation of runoff and soil erosion

The predicted cumulative discharges and sediment yields at the outlet of the basin during the 29 events were compared with the observed data (Table 5). Of all the simulations, the predicted and the observed values matched well and the model showed no consistent tendency to underestimate or overestimate runoff or soil erosion. Based on the simulated discharge results during the calibration phase and validation phase, the model performed better during the calibration phase (R^2=0.95) than in the validation phase (R^2=0.90) (Fig. 5). The *Nash* coefficients of efficiency were also calculated for each individual event, which varied from 90.3 to 94.2% for the

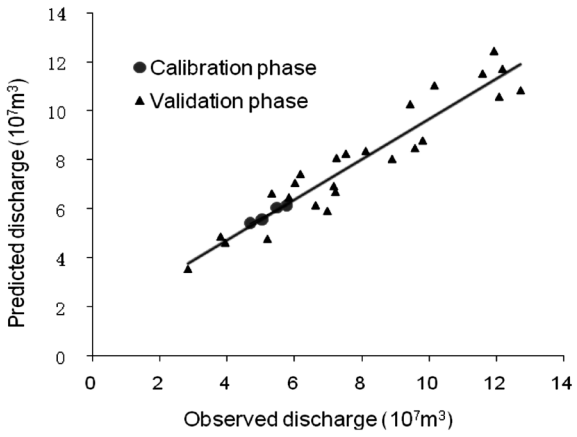

Fig. 5. Comparison between the simulated and observed river discharges during 29 events.

Table 3. Range of parameter values results from model calibration

Parameter	Symbol	Value range
Decay factor	m_0	0.01~0.1
Manning's coefficient	n_0	0.05~0.5
Maximum water storage of root zone	S_{rmax}	0.01~0.05
Transmissivity coefficients	D_{sand}, D_{silt}, D_{clay}	0.05~2.0
Saturated hydraulic conductivity	K_s	0.0325~0.0851

Table 4. *C* factor values calibrated for different land use types in the Lushi Basin

Forest	Shrub forest	Sparse forest	High–coverage grassland	Middle–coverage grassland	Low–coverage grassland	Farmland	Hill farmland
0.1	0.22	0.32	0.12	0.18	0.32	0.35	0.33

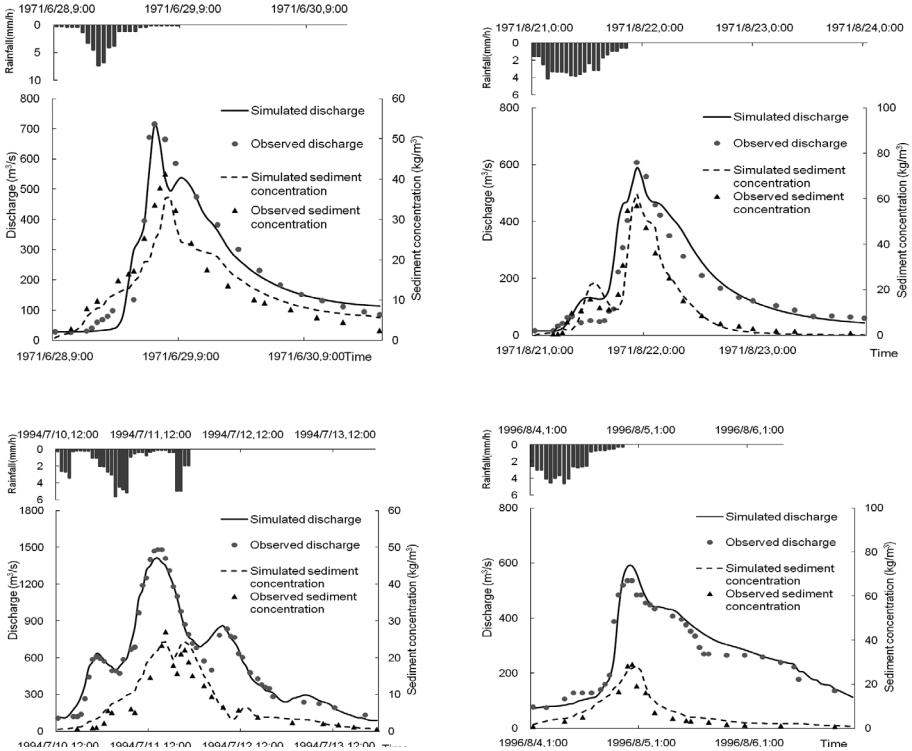

Fig. 6. Hydrographs of the four selected events during model calibration and validation.

Table 5. Observed and predicted runoff discharges and sediment yields at the basin outlet

Date	Runoff ($10^7 m^3$)		Deviation (%)	Sediment Yield (10^7 kg)		Deviation (%)
	Observed	Predicted		Observed	Predicted	
06/28/1971	6.77	6.13	9.5	23.36	24.90	6.6
08/21/1971	5.47	6.05	10.6	14.47	13.53	6.5
07/08/1972	5.03	5.86	16.5	12.14	12.57	3.5
06/30/1973	4.69	5.42	15.6	14.73	18.18	23.4
04/24/1975	6.97	5.91	15.2	15.25	16.82	10.3
08/22/1976	11.92	12.43	4.3	44.63	51.01	14.3
07/11/1979	3.94	4.61	17.0	18.16	20.99	15.6
07/31/1979	7.24	8.07	11.5	34.44	38.81	12.7
06/30/1980	10.15	11.03	8.7	70.02	66.39	5.2
07/15/1981	8.11	8.35	3.0	14.7	16.72	13.7
08/22/1981	6.17	7.41	20.1	29.57	33.32	12.7
08/14/1982	5.19	4.77	8.1	6.17	6.71	8.8
08/30/1982	6.62	6.14	7.3	21.56	24.44	13.3
06/24/1983	8.89	8.03	9.7	23.72	26.08	9.9
07/20/1983	9.8	8.78	10.4	49.82	46.22	7.2
08/03/1983	9.57	8.47	11.5	50.7	56.56	11.5
09/08/1983	7.16	6.92	3.4	32.48	31.04	4.4
07/06/1984	11.58	11.51	0.6	51.74	56.93	10.0
07/18/1984	5.83	6.46	10.8	32.75	38.95	18.9
06/05/1987	7.52	8.24	9.6	13.27	11.51	13.3
07/10/1989	12.71	10.83	14.8	55.4	51.30	7.4
08/18/1989	7.21	6.68	7.4	26.56	25.05	5.7
09/15/1991	2.83	3.54	25.1	6.64	8.19	23.3
08/13/1992	5.32	6.62	24.4	16.5	19.63	18.9
07/08/1994	6.01	7.05	17.3	31.74	34.49	8.7
07/10/1994	12.07	10.57	12.4	75.06	72.15	3.9
08/13/1995	3.8	4.86	27.9	30.19	34.78	15.2
08/04/1996	9.43	10.26	8.8	33.77	37.93	12.3
09/17/1996	12.17	11.7	3.9	61.1	63.47	3.9

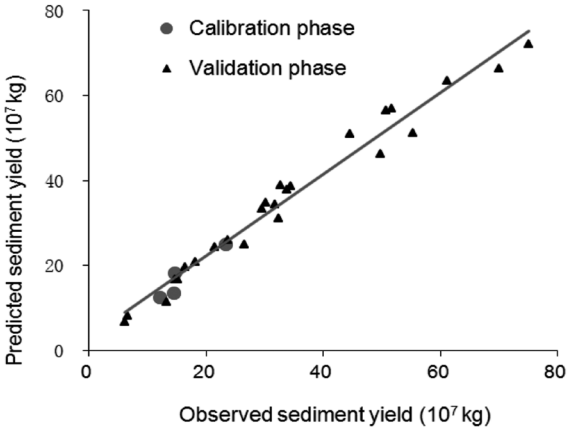

Fig. 7. Comparison between the simulated and observed river sediment concentrations during 29 events.

calibration phase and from 76.7 to 94.6% for the validation phase. The average *Nash* coefficients of efficiency derived for the calibration and validation phases were 92.8 and 90.7%, respectively. The four discharge hydrographs prepared during the calibration phase and validation phase demonstrate the model's ability to simulate the temporal variations in runoff during storm events (Fig. 6). The Nash coefficients for the events on June 28, 1971, August 21, 1971, July 10, 1994 and August 4, 1996 were 94.2, 90.3, 93.4% and 91.2%, respectively.

The averaged deviations of sediment yield simulations during the calibration and validation phases' were 10.0 and 11.2%, respectively (Table 5). Bingner *et al.* (1989) suggested that if the under–prediction or over–prediction of soil erosion was within 20% of the observed values, the simulation could be considered acceptable. On this basis, the simulated erosion results were generally within acceptable limits during the calibration and validation phases (Fig. 7). The predicted sediment yields showed a good match with the observed values during both the calibration phase (R^2=0.93) and the validation phase (R^2=0.91). The *Nash* coefficients of efficiency of soil erosion simulations varied in the range of 80.6% to 89.7% and 58.9% to 88.2% for the events during calibration and validation periods, respectively. The average Nash coefficient of efficiency of the 29 individual event simulations was about 70.4%. The sediment hydrographs for the events on June 28, 1971, August 21, 1971, July 10, 1994 and August 4, 1996 are provided in Fig. 6. The comparison between the simulated and observed sediment concentrations shows that the erosion model provided a good simulation of the overland soil loss and sediment outflow as long as the hydrological parameters generated from the rainfall–runoff model were accurate.

Spatial patterns of soil erosion and sediment deposition

The spatial distribution of soil erosion and deposition were analyzed for the selected events to investigate trends in erosion/deposition distribution, which was helpful in identification of areas prone to erosion in the study area. Net erosion patterns for different events were calculated by subtracting the deposition rates for each grid cell from the gross erosion rates for the corresponding grid cell. The net erosion estimated on a grid basis for the basin was grouped into the following erosion classes in this study: slight (0 to 10 t km^{-2}), moderate (10 to 20 t km^{-2}), high (20 to 40 t km^{-2}), very high (40 to 80 t km^{-2}) and severe (>80 t km^{-2}). The map for deposition of sediment for the event of July 10, 1994 (Fig. 8) shows negative values on the soil erosion map for areas where sediment deposition occurred (i.e. true sediment deposition), whereas positive values corresponded to grid cells with net soil erosion. The erosion map indicates severely eroded areas were mainly located in the region with poor vegetation cover and erodible soil properties. Statistics related to the above erosion classes are presented and classified into the percentage of area, slope and land use composition in the Lushi Basin for the selected event in Table 6. About 61.4% of the entire basin was found to be experiencing net erosion, among which the high erosion class encompass the largest percentage of the area. The areas with severe erosion class covered only 0.19% of the basin area and mainly included grids slopes of more than 25 degrees, but these severely eroded grids were the main erosion sources during all the simulated events. The erosion levels were closely related with slopes and areas with slight erosion had smaller average slopes than severely eroded areas (Table 6). Net deposition areas had an average slope of about 7 degrees and the areas with net erosion had an average slope of about 14 degrees, which revealed that soil erosion in the study area was tightly affected by topographic features. Detailed analysis related to land use composition and the distribution of soil erosion indicated that severely eroded areas were mainly located in the regions with poor vegetation cover and erodible soils. Sediment is usually deposited on areas of flatter slopes with dense vegetation cover. The net erosion areas had larger percentages of farmlands and low grassland coverage, while the net deposition areas had larger percentages of forest and high–coverage grassland (Table 6). This verified that grids with forest and high–coverage grassland land–use types generally had less soil erosion and more deposition, while grids with farmlands and low–coverage grassland land–use types were the main sources of soil erosion. Of all

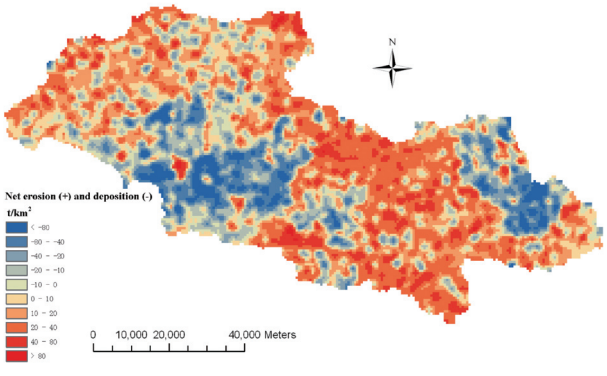

Fig. 8. Spatial distribution of soil erosion/deposition during the event of 10 July 1994

Table 6. Statistics related to the percentage of area, slope and land use composition of grids in the Lushi Basin

Statistics	< –80 (t km^{-2})	–80 – –40 (t km^{-2})	–40 – –20 (t km^{-2})	–20 – –10 (t km^{-2})	–10 – 0 (t km^{-2})	0 – 10 (t km^{-2})	10 – 20 (t km^{-2})	20 – 40 (t km^{-2})	40 – 80 (t km^{-2})	> 80 (t km^{-2})
Percentage of area	3.74%	9.87%	8.88%	6.79%	9.32%	12.89%	17.71%	23.85%	6.75%	0.19%
Slope (degree)	3.92	5.85	8.29	9.39	10.75	11.74	12.93	13.49	13.88	14.22
Forest	37.65%	36.95%	38.06%	39.37%	32.50%	21.61%	15.45%	9.15%	2.74%	0.86%
Shrub forest	5.88%	7.91%	6.55%	10.25%	7.61%	6.38%	4.71%	2.86%	1.60%	1.93%
Sparse forest	17.65%	18.27%	20.57%	11.40%	8.40%	7.83%	6.94%	4.70%	4.16%	1.13%
High–coverage grassland	5.88%	6.14%	4.86%	6.34%	7.31%	7.53%	8.68%	6.42%	2.62%	0.48%
Middle–coverage grassland	10.00%	6.99%	9.31%	10.76%	15.09%	18.78%	19.34%	18.87%	12.14%	9.00%
Low–coverage grassland	2.94%	3.37%	4.69%	4.55%	6.56%	8.43%	10.33%	13.91%	17.10%	20.4%
Hill farmland	15.00%	17.42%	14.83%	16.18%	20.12%	25.83%	29.83%	39.14%	50.63%	54.3%
Farmland	5.00%	2.95%	1.14%	1.15%	2.41%	3.61%	4.71%	4.96%	9.01%	11.9%

land use types, farmlands were major sources of soil erosion; and forests had the largest areas of deposition. Land use changes, especially between farmlands and forests, were shown to have important impacts on soil erosion in the Lushi Basin.

Effects of land use changes on soil erosion

Land use patterns, or the spatial structure of different land units, have an impact on soil erosion and sedimentation. For example, an increase in farmland area normally leads to a higher soil erosion risk. To explicitly evaluate the effects of land use change on soil erosion, the land use transition matrix was used to show the land use change between 1990 and 1995. The transition matrix of land use change processes in Lushi Basin from 1990 to 1995 was obtained (Table 7). The total forested area decreased by 10% from 1990 to 1995, while the areas of grassland and farmland increased by 6.7 and 3.3%, respectively, a total area of land use change between covering about 787.3 km^2. Changes mainly involved forests with about 461.8 km^2 of forested land being transformed into farmland and grass land. The newly cultivated farmland was mainly located in an area of the downstream plain near Lushi Station that was suitable for agricultural activities. To examine the soil erosion variations caused by different land use maps, four events recorded on July 10, 1989 (Storm 1), August 18, 1989 (Storm 2), August 4, 1996 (Storm 3) and September 17, 1996 (Storm 4) were selected for comparison because these four storm events included time periods which were close to the points in time used for the land use maps. These were also selected because the cumulative rainfalls and total runoff volumes are similar between the two pairs of events, Storm 1 and Storm 4, Storm 2 and Storm 3 (Table 5), which excluded the interference of different rainfalls on analyzing the impact of land use changes on soil erosion. The durations of the selected four events were all about 72 hours and the spatially averaged peak rainfall intensities recorded during the four events were all within the range of 10.0–12.0 mm h^{-1}. The similar cumulative rainfalls and peak rainfall intensities between the two pairs of storm events (Storm 1 and Storm 4, Storm 2 and Storm 3) caused similar erosivity R factors. Therefore, the significant influences of R fac-

Table 7. Transition matrix of land use change processes in Lushi Basin from 1990 to 1995 (km^2)

Land use type	Forest	Shrub forest	Sparse forest	High–coverage grassland	Middle–coverage grassland	Low–coverage grassland	Hill farmland	Farmland	1990 total	Ratio (%)
Forest	182.3	25.8	23.7	63.1	157.8	13.8	49.8	143.0	1659.3	37.5
Shrub forest	4.9	279.6	2.0	7.9	1.5	0.3	4.0	2.0	302.2	6.8
Sparse forest	1.8	4.7	470.4	5.7	5.7	3.0	7.6	8.4	507.3	11.5
High–coverage grassland	3.0	4.4	1.0	242.6	5.3	2.4	3.6	2.1	264.4	6.0
Middle–coverage grassland	2.6	4.2	2.3	13.9	381.5	48.0	10.8	3.9	467.2	10.6
Low–coverage grassland	0.6	0.7	0.5	6.6	6.7	332.2	11.6	0.8	359.7	8.1
Hill farmland	0.8	2.0	3.4	7.0	20.6	57.9	418.1	11.8	521.6	11.8
Farmland	1.4	1.8	0.4	2.2	1.5	1.0	3.6	329.1	341.2	7.7
1995 total	1197.6	323.3	503.7	349.1	580.6	458.4	509.2	501.2	4423.0	100.0
Ratio (%)	27.1	7.3	11.4	7.9	13.1	10.4	11.5	11.3	100.0	

Table 8. Contributions of different land use types to soil erosion or deposition in the Lushi Basin

Land use type	Area changesbetween two years (km^2)	Total contributions to soil erosion (+) or deposition (–) in the basin		Average soil erosion (+) or deposition (–) on a grid cell (kg)	
		1989	1996	1989	1996
Forest	–461.8	–85.06%	–72.18%	–1941.7	–1756.2
Shrub forest	+21.04	6.87%	6.04%	+881.4	+803.9
Sparse forest	–3.62	21.65%	18.72%	+1654.3	+1597.3
High–coverage grassland	+84.62	–12.46%	–20.22%	–1785.3	–1687.3
Middle–coverage grassland	+113.47	–3.64%	–6.12%	–294.9	–307.1
Low–coverage grassland	+98.65	13.15%	14.60%	+1417.3	+1369.5
Hill farmland	–12.36	43.19%	39.14%	+3210.1	+3304.7
Farmland	+160.0	16.11%	21.35%	+1829.1	+1831.4

tors on final soil loss were excluded from the comparison. Meanwhile, the *K, L, S* and *P* factors could be considered to be unchanged for the same basin, and thus land use changes played an important role in determining the soil loss and river sediment concentration through *C* factor. Soil erosion and deposition results over the whole Lushi Basin were summarized on the basis of land use types and the spatially averaged net erosion (or deposition) rates and total contributions to erosion (or deposition) of each land use type in 1989 and 1996 (Table 8). Differences between net erosion and deposition rates in the two years were not obvious with the deviations of these differences falling within a small range, 0.13–9.55%, and the average deviation was 4.73%. However, the temporally averaged sediment concentrations were estimated to be 4.57, 4.32, 6.91 and 7.36 kg m^{-3} at the outlet for the Storms 1, 2, 3 and 4, respectively. This implied that the averaged sediment concentration during the storm events recorded in 1996 increased by 60.5% from the 1989 level. The results showed that a decrease in the percentage of forested land had generally led to an increase in the area of arable land prone to erosion, and that the erosion risk increased if a forest was transformed into farmland. The results also showed that low–coverage grassland and sparse forest were potential soil loss sources, and that appropriate management was needed to improve their environmental functions.

CONCLUSIONS

In this paper, an integrated erosion model was presented that was developed based on the distributed hydrological model and applied to assist in assessing the impact of land use changes on soil erosion potential. Through a case study in Lushi Basin between 1971 and 1996, the model gave good results in simulating river discharge, soil erosion and sediment transport at hourly time intervals. The comparison of two historical land use maps showed that some parts of the Lushi Basin experienced deforestation and increased agricultural activities and associated land degradation, which altered the total erosion amount and the average erosion rate. The reason is that the responses of soil erosion and sediment delivery to land use changes were non–linear, a small change in landscape results in relatively large changes in erosion risk and sediment delivery. Also, sediment delivery was more sensitive to land use changes than soil erosion because of the sediment trapping effect of forested areas. Through the grid–based distributed modeling, it was found that not only the composition but also the spatial position of land use parcels were similarly important in soil erosion. The model supplies a tool supporting integrated management practices in a meso–scale river basin.

ACKNOWLEGEMENTS

This research is supported by the National Natural Science Foundation of China (Grant No. 41001155) and Program for New Century Excellent Talents in University (NCET–12–0058).

REFERENCES

Ao T. Q., K. Takeuchi and H. Ishidaira 2000 On problems and solutions of the Muskingum–Cunge routing method applied to a distributed rainfall runoff model (in Japanese). *Ann. J. Hydraul. Eng. (JSCE)*, **44**: 139–144

Ao T. Q., K. Takeuchi and H. Ishidaira 2001 On the method of generating artificial stream networks of large river basins and its effect on runoff simulation (in Japanese). *Ann. J. Hydraul. Eng. (JSCE)*, **45**: 139–144

Beasley D. B., L. F. Huggins and E. J. Monke 1980 ANSWERS: a model for watershed planning. *Trans ASAE*, **23**: 938–944

Beven K. J., R. Lamb, P. Quinn, R. Romanovicz and J. Freer 1995 TOPMODEL. *In: Signh VP Computer models of watershed hydrology, Water Resources Publications, Highlands Ranch*, pp. 627–668

Bryan R. B and J. Poesen 1989 Laboratory experiments on the influence of slope length on runoff, percolation andrill development. *Earth Surface Processes and Landforms*, **14**: 211–231

Bingner R. L., C. E. Murphee and C. K. Mutchler 1989 Comparison of sediment yield models on various watersheds in Mississippi. *Trans ASAE*, **32**: 529–534

Chou W. C. 2010 Modelling watershed scale soil loss prediction and sediment yield estimation. *Water Resour. Manage*, **24**: 2075–2090

Daniel G. Y., A. W. Glenn, K. M. Donalad, C. M. Keith and L. B. Ronald 2003 User's guide: *Revised Universal Soil Loss Equation Version 2 –RUSLE2*

Desmet P. J. and G. Govers 1966 A GIS procedure for automatically calculating the USLE LS factor on topographically com-

plex landscape units. *J. Soil and Water Conservations* **51**: 427–433

Dunjo G., G. Pardini and M. Gispert 2004 The role of land use–land cover on runoff generation and sediment yield at a microplot scale, in a small Mediterranean catchment. *J. Arid Environ.*, **57**: 99–116

Favis–Mortlock D. and J. Boardman 1995 Nonlinear responses of soil erosion to climate change: a modelling study on the UK South Downs. *Catena*, **25**: 365–387

Hao F. H., X. S. Zhang, H. G. Cheng, C. M. Liu and Z. F. Yang 2004 Runoff and sediment yield simulation in a large basin using GIS and a distributed hydrological model. *IAHS Publ.*, **289**: 157–166

Houben P, T. Hoffmann, A. Zimmermann and R. Dikau R 2006 Land use and climatic impacts on the Rhinesystem RheinLUCIFS): Quantifying sediment fluxesand human impact with available data. *Catena*, **66**: 42–52

Jain M. K. and D. Das 2010 Estimation of sediment yield and areas of soil erosion and deposition for watershed prioritization using GIS and remote sensing. *Water Resour. Manage.*, **24**: 2091–2112

Jordan G., A. van Rompaey, P. Szilassi, G. Csillag, C. Mannaerts and T. Woldai 2005 Historical landuse changes and their impact on sediment fluxes in theBalaton basin (Hungary). *Agr. Ecosys. Environ.*, **108**: 119–133

Kinnell P. I. A. 1997 Runoff ratio as a factor in the empirical modeling of soil erosion by individual rainstorms. *Aust. J. Soil*, **35**: 1–13

Kinnell P. I. A. 2003 Event erosivity factor and errors in erosion predictions by some empirical models. *Aust. J. Soil*, **41**: 991–1003

Kinnell P. I. A. 2005 Alternative approaches for determining the USLE–M slope length factor for grid cells. *Soil Science Society of America Journal*, **69**: 674–680

Ludwig B., J. Boiffin, J. Chadoeuf, A. V. Auzet 1995 Hydrological structure and erosion damage caused by concentrated flow in cultivated catchments. *Catena*, **25**: 227–252

Morgan R. P. C., J. N. Quinton, R. E. Smith, G. Govers, J. W. A. Poesen, K. Auerswald, G. Chisci, D. Torri and M.E. Styczen 1998 The European Soil Erosion Model (EUROSEM): A dynamic approach for predicting sediment transport from fields and small catchments. *Earth Surface Processes and Landforms*, **23**: 527–544

Nash J. E. and J. V. Sutcliffe 1970 River flow forecasting through conceptualmodels: Part I–A discussion of principles. *J. Hydrol.*, **10**(3): 282–290

Nearing M. A., L. J. Lane and V. L. Lopes 1994 Modeling soil erosion. In: *Lad R, Soil Erosion: Research Methods*, pp. 127–156

Ni J. R., X. X. Li and A. G. L. Borthwick 2008 Soil erosion assessment based on minimum polygons in the Yellow River basin, *China. Geomorphology*, **93**: 233–252

Nicks A. D., R. D. Williams and G. A. Gander 1994 Estimating the impacts of global change on erosion with stochastically generated climate data and erosion models. In Variability in stream erosion and sediment transport: proceedings of an international symposium held at Canberra, Australia, 12–16 December 1994. p. 498. Edited by L. J. Olive, R. J. Loughran and J. A. *Kesby. IAHS Publication* 224

Philip J. R. 1957 The theory of infiltration: 1. The infiltration equation and its solution. *Soil Sci.*, **83**: 435–448

Pruski F. F. and M. A. Nearing 2002 Runoff and soilloss responses to changes in precipitation: A computersimulation study. *J. Soil Water Cons.*, **57**: 7–16

Renard K. G. and G. R. Foster *et al*. 1997 Predicting soil erosion by water: a guide to conservation planning with the revised universal soil loss equation (RUSLE), *Agricultural handbook*, No. 703. USDA, Washington

Ricker M. C., B. K. Odhiambo and J. M. Church. 2008 Spatial analysis of soil erosion and sediment fluxes: A paired watershed study of two Rappahannock river tributaries, Stafford county, Virginia. *Environ. Manage.*, **41**: 766–778

Risse L. M., M. A. Nearing, A. D. Nicks and J. M. Laflen JM. 1993 Error assessment in the Universal Soil Loss Equation. *Soil Sci. Soc. Am. J.*, **57**: 825–833

Romkens M. J. M., K. Helming and S. N. Prasad 2001 Soil erosion under different rainfall intensities, *surface roughness, and soil water regimes. Catena*, **46**: 103–123

Sharma A., K. N. Tiwari and P. B. S. Bhadoria 2011 Effect of land use land cover change on soil erosion potential in an agricultural watershed. *Environ. Monit. Assess*, **173**: 789–801

Singh R. K., R. K. Panda, K. K. Satapathy and S. V. Ngachan 2012 Runoff and sediment yield modelling for a treated hilly watershed in eastern Himalaya using water erosion prediction project model. *Water Resour. Manage.*, **26**: 643–665

Sherman L. K. 1943 Comparison of F–curves derived by the methods sharp and Holtan and of Sherman and Mayer. *Trans AGU*, **24**: 465–467

Takeuchi K., T. Q. Ao and H. Ishidaira 1999 Introduction of block–wise use of TOPMODEL and Muskingum–Cunge method for the hydro–environmental simulation of a large ungauged basin. *Hydro. Sci., J* **44**: 633–646

Toy J. T., G. R. Foster and K. G. Renard 2002 Soil erosion. Processes, prediction, measurement, and control. *Hoboken*: Wiley

Wang G. Q., M. C. Zhou, K. Takeuchi and H. Ishidaira 2007 Improved version of BTOPMC model and its application in event–based hydrologic simulations. *J. Geo. Sci.*, **17**: 73–84. doi:10.1007/s11442–007–0073–2

Wang G. Q., H. A. P. Hapuarachchi, K. Takeuchi and H. Ishidaira 2010 Grid–based distribution model for simulating runoff and soil erosion from a large–scale river basin. *Hydrol. Process.*, **24**: 641–653

Wischmeier W. H. and D. D. Smith 1978 *Predicting rainfall erosion losses*. USDA Agricultural Research Services Handbook 537. USDA, Washington, DC, p. 57